

Chapter 6

Line Feed Design

The results from this chapter are published as: Leung, M., Kot, J.S. and Jones, B.B. 'Wideband Dual Polarised Line Feed for a Cylindrical Reflector Radio Telescope.' June, 2007. IEEE Antennas and Propagation International Symposium. pp. 1929–1932.

A key component of the Square Kilometre Array Prototype (SKAMP) upgrade to the Molonglo Observatory Synthesis Telescope (MOST) is the new line feed. This feed will enable polarisation capability, increased observing frequency range and improve the overall system sensitivity for the current MOST operation. Design specifications for the new line feed were established in Chapter 3, and used in Chapter 4 to select the wideband dipole as the preferred design. Reflector simulations in Chapter 5 showed the half-power beamwidth range, 70° – 100° , would provide optimum aperture efficiency and minimise spillover temperature for the given reflector geometry. This chapter describes the design methodology and presents simulations of the feed performance.

Analytical methods used to model the array performance are described in Section 6.1. A full-wave electromagnetic (EM) analysis of the array is needed to account for mutual coupling between array elements. The selection of an EM solver used to analyse the array is presented in Section 6.2. Although a wideband dipole element was selected (Section 4.2) and dual linear is the polarisation (Section 3.3.4), the array configuration has not been determined. Section 6.3.1 describes the selection of a particular array configuration for the line feed. A novel feeding technique is presented in Section 6.3.2. Simulated transverse plane element patterns are presented in Section 6.4.1. Beamwidth matching for the two polarisations is investigated in Section 6.4.2. Transverse plane element patterns are presented in Section 6.4.3. Simulated gain variation with scan angle in the longitudinal plane is presented in Section 6.4.4. Impedance models are discussed in Sections 6.4.5 and Section 6.4.6.

6.1 Array Analysis Methods

Before investigating the element design, the effect of mutual coupling between elements in an array is considered, as this limits the overall performance. Two key parameters used to determine the array performance are the scan element pattern and the scan impedance. The theory presented in this section follows from Hansen (1998).

6.1.1 Scan Impedance and Element Pattern

The impedance at the feed point for elements in an array will vary as a function of scan angle because of a changing mutual coupling environment. For a finite array, the impedance of the centre elements in the array may differ from the edge elements. The analysis presented here will assume the array is infinitely long, such that identical impedance is seen at each element. This assumption is valid for the MOST line feed which is over 778 m in length, being $> 2000\lambda$ at its operating frequency. For a given scan angle, θ , the scan impedance, $Z_s(\theta)$, is generated by applying the correct amplitude and phase to each element as shown in Figure 6.1(a). The scan impedance is related to the scan reflection coefficient, $\Gamma_s(\theta)$, by:

$$\Gamma_s(\theta) = \frac{Z_s(\theta) - Z_0}{Z_s(\theta) + Z_0} \quad (6.1)$$

Where Z_0 is the impedance of the generator feeding the antenna elements. The scan impedance affects the array performance through a mismatch factor $(1 - |\Gamma_s(\theta)|^2)$. The array pattern performance, $G(\theta)$, is obtained by multiplying the isotropic array factor, AF , by the single element pattern in isolation, g_{iso} , and the impedance mismatch factor:

$$G(\theta) = AF g_{iso}(\theta) (1 - |\Gamma_s(\theta)|^2) \quad (6.2)$$

Where the array factor for a line feed is:

$$AF = \sum_{n=0}^{N-1} I_n e^{jkm d \cos \theta} \quad (6.3)$$

Where I = current magnitude

d = element spacing

$k = 2\pi/\lambda$ (wavenumber)

N = number of array elements

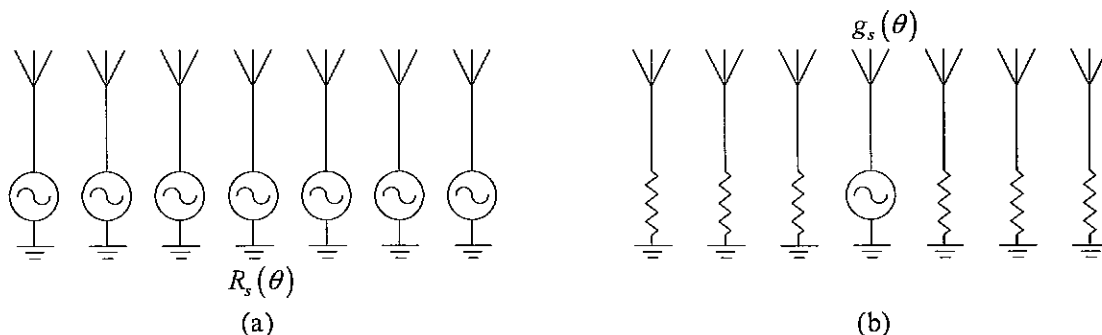


Figure 6.1 (a) Scan impedance array excitation. (b) Scan element pattern array excitation

Direct measurement of the scan impedance is difficult because it requires modification of the complete phasing network used to scan the array (Pozar 1994; Hansen 2001). A more common approach is to assume an infinite array environment using a unit-cell technique.

Measurements with specialised hardware such as waveguide simulators are used to verify the results (Hansen 2001). In the present case, the unit-cell technique is used to determine the scan impedance seen at the feed point (Section 6.4.6), with the results being indicative of the performance. Furthermore, the effect of the balun is not considered. Instead, the design approach concentrates on modelling the impedance of a single element (Section 6.4.5) and matching the impedance at 0° scan angle. This approach was taken because the performance of a single element is indicative of the array performance and no specialist phasing network was required for testing at 0° scan angle. In addition, it is difficult to minimise the impedance mismatch factor by matching the antenna scan impedance to the generator impedance across a wide bandwidth, because of the large scan impedance variation. Flexibility was designed into the antenna matching network, described in Section 7.1.2, so that the antenna impedance could be modified if required in the future.

The scan element pattern is used to characterise the array gain variation with scan angle in the plane of measurement. The array pattern performance is calculated by multiplying the isotropic array factor and the scan element pattern, $g_s(\theta)$:

$$G(\theta) = AF g_s(\theta) \quad (6.4)$$

To measure the scan element pattern, one element must be properly excited and the other elements in the array terminated in matched impedances, as shown in Figure 6.1(b). Mutual coupling effects from surrounding elements are included and the array polarisation performance can be determined by a cross-polar measurement. The scan element pattern is related to the scan impedance and the isolated element pattern (Hansen 1998):

$$g_s(\theta) = \frac{R_{iso} g_{iso}(\theta)}{R_s(\theta)} \left(1 - |\Gamma_s(\theta)|^2\right) \quad (6.5)$$

When the generator is matched to the scan resistance at $\theta = 0^\circ$, this gives:

$$g_s(\theta) = \frac{R_s(0) g_{iso}(\theta)}{R_s(\theta) g_{iso}(0)} \left(1 - |\Gamma_s(\theta)|^2\right) \quad (6.6)$$

The array performance can be analysed using the scan impedance and scan element pattern. Both parameters may exhibit nulls or resonances at particular scan angles and frequencies. A null in the scan element pattern could indicate a blind angle, where the array radiates or receives no signal. These are generated when the array supports a surface wave which cancels out the radiation in a particular direction. Surface waves come from the type of element and array geometry used. Techniques to minimise these effects are discussed in Hansen (1998). Resonances appearing in the scan impedance at a particular scan angle and frequency can also indicate problems in the element design and array configuration. For example, a scan impedance resonance may occur at a scan angle if there is an unwanted asymmetric mode in the feed network. Similarly, a 'bad' element design or layout may generate increased coupling between polarisations or insufficient grounding for the feed network that could cause a resonance. Locating these blind angles

and resonances by using the scan element pattern and scan impedance is necessary, so the design may be modified.

6.2 Solver Selection

Simulations for the feed design provide the scan element pattern and scan impedance. These are electromagnetic (EM) parameters, so a full-wave EM simulation is required. Solution options involve developing a customised 3D EM code for the wideband dipole element or adaptation of a commercial EM software package.

Technology growth in the electronics industry has been paralleled with an increase in commercially available 3D EM software packages used to model electrical components. As electronic components are operating at faster speeds and circuit miniaturisation is employed, standard empirical models become inadequate and an EM analysis is necessary to model the coupling or cross-talk between different parts of the circuit. Computer Simulation Technology's Microwave Studio (CST MWS) was the selected software package for the present work.¹ Compared to other 3D EM solvers, it uses the finite integration technique (FIT) to transform the integral form of Maxwell's equations into an equivalent pair of dual interlaced Maxwell grid equations (Lau et al. 2005). This enables a time-domain FIT to be applied to a Cartesian grid, which is similar to the finite difference time domain method (FDTD; Stutzman and Thiele 1998). A key difference is that MWS uses a perfect boundary approximation (<http://www.cst.com>) to model curved geometries rather than the staircase approximation used in most FDTD approaches. This gives improved accuracy when modelling complex antenna geometries. The time-domain FIT enables all the frequency-domain data to be calculated from a single time-domain simulation through a Fourier transform. This method is faster for the wideband line feed design, where the element pattern must be analysed at many frequency points across the band, as presented in Sections 6.4.1 to 6.4.4.

A unit-cell approach is used for calculating the scan impedance, as described in Section 6.1.1. This requires periodic boundary conditions to be placed at the element spacings where the array is assumed to be infinite in extent. The time-domain solver enables the use of periodic boundaries. However, the calculation technique used does not permit the application of a periodic phase shift or scan angle. A periodic phase shift is required to represent the condition in Figure 6.1(a), where all the line feed elements are phased to a particular scan angle. By assuming a time-harmonic dependence of the EM fields, Maxwell's equations can be transformed into the frequency-domain. This transform is applied to the FIT to provide a frequency-domain solver option in MWS, which enables periodic phase shifts for a unit-cell and can model the scan impedance of the line feed design (Section 6.4.6). A disadvantage of the frequency-domain solver is that a single simulation is required for every frequency point and every scan angle, which increases simulation time.

¹ CST MWS simulation models developed in this chapter all used the standard mesh generation and solver accuracy settings unless stated otherwise.

6.3 Feed Analysis

The selected wideband dipole element is described in Section 4.2. It has a high degree of polarisation purity, low back radiation and cost effective engineering requirements. Dual linear polarisation (Section 3.3.4) produces the best performance compared to dual circular and slant polarisations and enables the transverse feed patterns to remain symmetrical on both polarisations as the feed is scanned. However, the patterns and input impedance for orthogonal polarisations in a dual linear line feed configuration are unequal, due to their orientation on the ground plane. An investigation is presented in Section 6.4.2 to match the co-polar transverse patterns on orthogonal polarisations. As discussed in Section 5.2, the line feed polarisations are called horizontal (HP) and vertical (VP) with respect to the array direction and are shown in Figure 5.2.

Although design specifications were presented in Table 3.6, some antenna parameters relating to the feed pattern and bandwidth were undefined at that point because the element type was not determined. Table 6.1 contains an updated set of line feed specifications. The impedance and radiation performance of the element in a line feed is determined by its array configuration and feeding technique, which are presented next.

Antenna Parameter	SKAMP Line Feed Specification
Design frequency range	500–1000 MHz
Centre frequency (λ_c)	866 MHz
Feed beam pattern (HPBW)	70°–100°
Front-to-back-ratio (F/B)	> 25 dB
Polarisation sensitivity	0.05 (–26 dB)
Impedance bandwidth	1.7:1
Return loss (dB)	–10 dB
Scanning bandwidth	1.5:1
Pattern bandwidth	1.7:1
Angular scan range	±60°
Element size	0.33 λ_c
Element height above ground plane	0.25 λ_c

Table 6.1 Wideband dipole element specifications for the SKAMP feed.

6.3.1 Array Configuration

A wideband dipole element can be arranged in different array configurations to measure dual linear polarisation. Factors influencing the performance of the particular configuration are mutual coupling between array elements, scanning bandwidth, ease of implementation and transverse feed pattern symmetry. Although there are several configurations that can produce dual linear polarisation, three potential choices are shown in Figure 6.2: a line feed with elements arrayed along the arm diagonal as in Figure 6.2(a), elements arrayed along the arm width in Figure 6.2(b) and elements arrayed with their polarisations offset with respect to the phase centre line in Figure 6.2(c).

When the feed polarisations are offset from the centre of the ground plane, as in Figure 6.2(c), the transverse patterns will be asymmetric for both orthogonal polarisations. Furthermore, scanning the beam causes a beam centre shift and skewed patterns. This produces an uneven reflector illumination, resulting in a reflector pattern pointing error

and defocusing effects. Line feed configurations in Figures 6.2(a) and 6.2(b) have their polarisations aligned with the ground plane centre line and exhibit no beam centre variation or skewing in the transverse patterns. The physical gap between arrayed elements in Figure 6.2(b) is greater than for those in Figure 6.2(a), for the same fixed array spacing. A larger gap minimises mutual coupling effects. However, to maximise the scanning bandwidth, closer element spacing is preferred, as can be achieved using the configuration in Figure 6.2(b). The design complexity to implement dual linear polarisation with this configuration may be greater compared to the Figure 6.2(a) configuration. This is because elements in the Figure 6.2(a) configuration are fed across the arm diagonal, which can be achieved using a typical crossed dipole feeding method (Section 4.1.2). Nevertheless, the array configuration in Figure 6.2(b) is preferred because of the larger scanning bandwidth. A novel method to excite dual linear polarisation using this configuration was discovered and is described next.

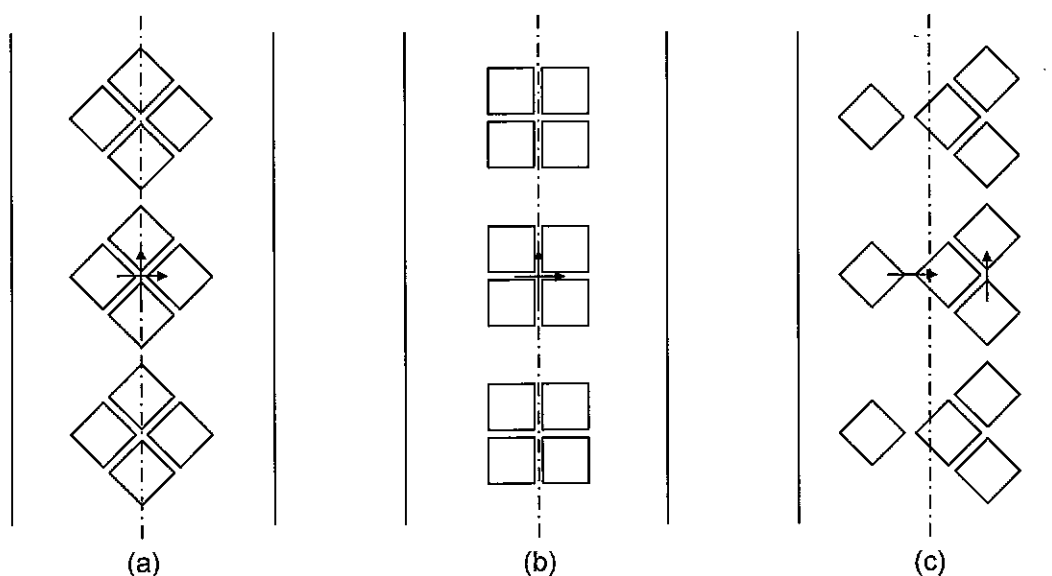


Figure 6.2 Line feed array configurations. (a) Along the arm diagonal. (b) Along the arm width. (c) Offset from the centre line.

6.3.2 Feeding Method

To generate dual linear polarisation for the line feed array configuration shown in Figure 6.2(b), a new feeding method is necessary, different from techniques used in existing wideband dual polarised dipole designs by Suh et al. (2003), Perruisseau-Carrier et al. (2003) and Wong and King (1972). In these examples, the wideband dual polarised dipole arms are fed across the diagonal dimension, i.e. arms A-D and B-C (see Figure 6.3). Whereas, the selected array configuration requires feeding the dipole arms across the width dimension AC-BD and AB-CD. This is realised by considering the wideband dipole as four separate dipoles: A-B, C-D, A-C and B-D, which are then fed in pairs to excite the correct polarisation. This method is called the feeding in-pairs technique and is shown in Figure 6.3, where an equal magnitude and in-phase voltage, V_1 , is applied across arms A-B and C-D to generate vertical polarisation and similarly, an equal magnitude and in-phase voltage, V_2 is applied across arms A-C and B-D to generate horizontal polarisation.

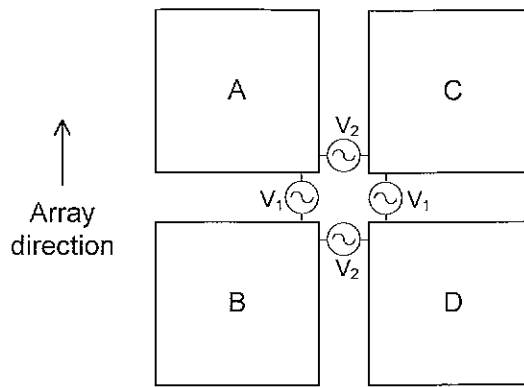


Figure 6.3 Top view of wideband dual polarised dipole element, showing feeding in-pairs.

The voltage across the arms can be generated using two different methods, as described in Section 4.1.2. The first method uses a hybrid coupler connected across the arms to provide the correct excitation and the second method uses a balun feed. Although both methods create the desired voltage excitation, the hybrid coupler is rejected because it is more expensive, with higher noise temperature due to losses. Because the wideband dipole is considered as four separate dipoles, four baluns are required. The top view in Figure 6.4 shows the use of four cable baluns, labelled 1 and 2 for the vertical polarisation and 3 and 4 for the horizontal polarisation, which are connected to the arms. Each balun consists of two cables, with a detailed description provided in Section 7.1.1. Outputs from each pair of baluns corresponding to the same polarisation are combined using a feed network below the ground plane to facilitate the equal amplitude and in-phase voltage excitation for the feeding in-pairs technique. This is shown in the side view in Figure 6.4 where VP and HP refer to vertical polarisation and horizontal polarisations respectively. The implementation of the feeding method for the dual polarised dipole is described in Section 7.1.

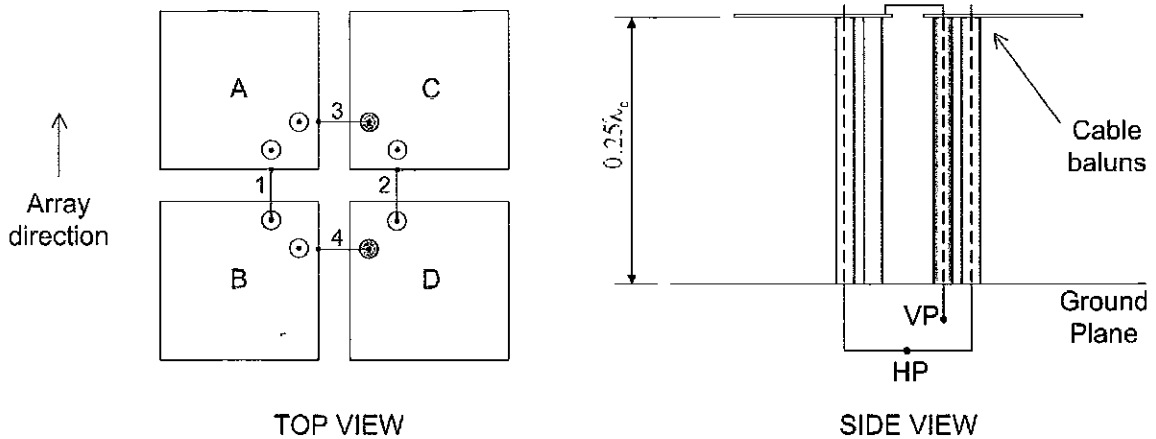


Figure 6.4 Element fed by four cable baluns with common inputs below ground plane to enable the in-pairs feeding.

6.3.3 Line feed Module

Section 3.1 discusses the two-stage RF beamforming architecture planned for SKAMP. This approach was taken to reduce the data processing volume. The first-stage beamformer will be connected to an 8-element line feed called a 'module'. Because the RF performance of the module governs the overall radiation characteristics of the

telescope, it is evaluated in this chapter. The 8-element module is around 1.5 m in length, with the elements spaced at $0.5\lambda_c$ (0.173 m) at a centre frequency of 866 MHz. Selecting an 8-element module enables the combination of 6 modules to form a 9 m length of line feed, connected to the second-stage beamformer. This feed length corresponds to a half-power beamwidth of around 2° in the longitudinal plane to match the transverse plane reflector beamwidth, therefore producing a symmetric imaging beam.

6.4 Line Feed Simulations

The chosen feed element is simulated to determine the radiation pattern and impedance performance, compared to the specifications in Table 6.1. Element pattern simulations are conducted to determine the radiation performance in transverse and longitudinal planes, depicted in Figure 6.5. One of the central elements in the array is fed and the other elements are terminated with resistive loads matched to the reference impedance. Element patterns in the transverse plane represent the feed radiation pattern that will illuminate the curvature of the reflector, whereas element patterns in the longitudinal plane represent the gain variation across the scan angle range. Radiation patterns for the line feed are presented in this chapter without the reflector because it is more efficient to optimise the line feed design separately from the reflector. Combined line feed and reflector patterns are presented in Chapter 8.

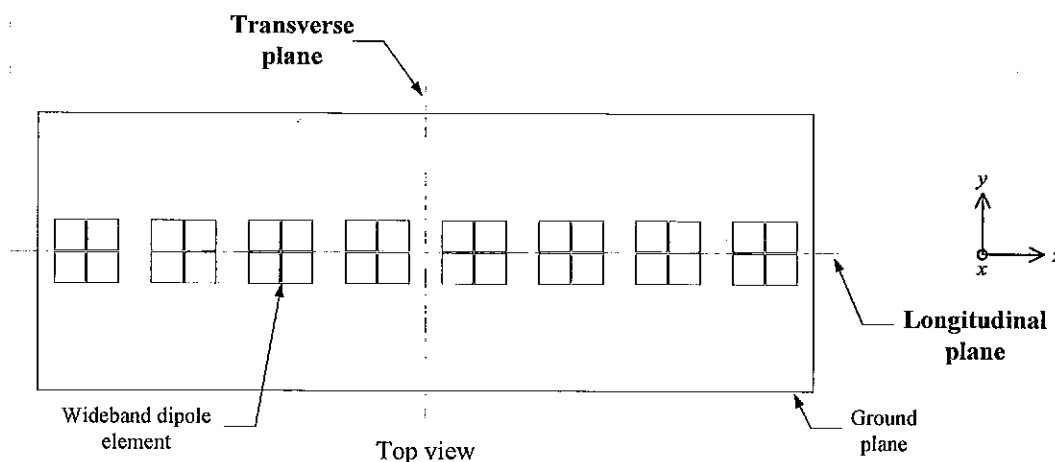


Figure 6.5 Line feed module with the element pattern planes defined.

Transverse plane pattern simulations are produced to determine whether the half-power beamwidth design goal of 70° – 100° is satisfied for both vertical and horizontal polarisations. Patterns are unequal for the two polarisations because of their alignment on the ground plane. A beamwidth matching method is investigated to produce approximately equal patterns for orthogonal polarisations. Simulations are presented for 0° scan angle in the design stages and then at 15° increments across the 0° – 60° range once the design has been optimised. Longitudinal plane element patterns are then presented for the optimised design. Radiation patterns are simulated at the centre frequency, 866 MHz and at 100 MHz intervals across the design frequency range of 500–1000 MHz. Once the element patterns for the line feed have been characterised, the input impedance of the feed is analysed. This analysis is initially carried out for a single element, which is generally predicative of array performance. Once the impedance performance of a single element has been modelled, it will be implemented in Section 7.1.2 and measured in an array environment in Section 7.2.3.

An 8-element module of wideband dual polarised dipoles is used in the element pattern simulations. The in-pairs feeding technique described in Section 6.3.2 is used to feed the elements, with a CST Microwave Studio model shown in Figure 6.6. Ideal voltage sources are placed across the arm gaps and simultaneous port excitation is used to generate the equal amplitude in-phase inputs. The use of an ideal voltage source means the practical effects of the balun are not modelled in the radiation pattern. The balun is omitted because it is electrically small compared to the dimensions of the line feed module. It is assumed that the balun provides an ideal voltage source across the dipole arms and has a negligible effect on the radiation patterns. However, the balun has a significant effect on the input impedance, which is investigated in Section 7.1.2. Due to difficulty in modelling the electromagnetic performance of the balun, it is characterised by a combination of empirical and experimental techniques.

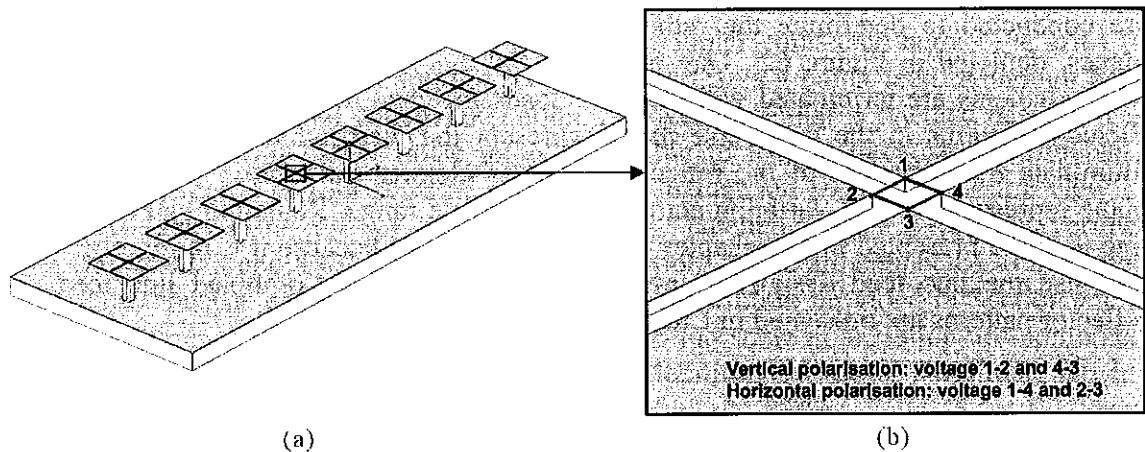


Figure 6.6 CST MWS model. (a) 8-element module. (b) Zoomed view of in-pairs feeding.

In the CST MWS simulations, the dipole arms were modelled as perfect electric conductors (PEC), without any dielectric materials. Dielectrics are used in the element construction and their effects on the electrical performance are minimised using a technique described in Section 7.1. The width of the ground plane in the transverse plane is fixed at 500 mm, as described in Section 3.4.1. The line feed model dimensions used for the element pattern simulation is shown in Figure 6.7.

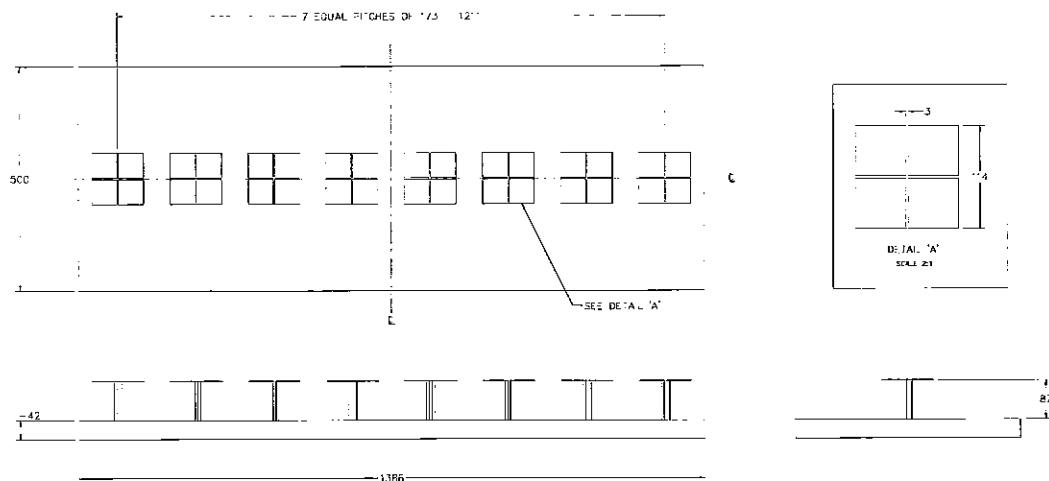


Figure 6.7 Mechanical drawing of 8-element module for CST MWS simulations. (Note dimensions in mm).

6.4.1 Transverse Plane Element Patterns

An 8-element array was simulated in CST MWS and parameters for vertical and horizontal polarisations at 0° scan angle are listed in Table 6.2. The cross-polar ratio (XPR) is calculated using Equation 3.17 across the reflector subtended half-angle range from -88° to +88° and is presented as the maximum XPR in this range. Parameters for the two polarisations are different, as expected from their respective orientations on the ground plane. This is shown in Figures 6.8(a) and 6.8(b) which compare the beamwidths and edge tapers. The difference in feed beamwidth for each polarisation across the frequency range is around 20°, with the horizontal polarisation narrower than the specified lower limit of 70° for frequencies < 925 MHz. The feed edge taper for the vertical polarisation remains relatively constant at -12 dB across the frequency range. There is a much larger variation for the horizontal polarisation, which varies up to 5 dB over particular 100 MHz instantaneous bandwidths intervals. Ideally the edge taper, should not vary across the bandwidth interval, in order to reduce the beamwidth variation in the reflector pattern and maintain a constant sensitivity.

Freq (MHz)	Vertical Polarisation				Horizontal Polarisation			
	HPBW (°)	Edge taper (dB)	F/B (dB)	XPR (dB)	HPBW (°)	Edge taper (dB)	F/B (dB)	XPR (dB)
500	84	-13	28	-25	60	-19	18	-8
600	90	-11	32	-28	60	-24	26	-11
700	85	-12	27	-28	57	-26	22	-17
800	85	-13	26	-28	61	-29	24	-11
866	92	-13	28	-30	65	-31	25	-7
900	95	-12	29	-32	68	-32	25	-5
1000	103	-12	31	-38	77	-35	25	-5

Table 6.2 Simulated pattern parameters for vertical and horizontal polarisations.

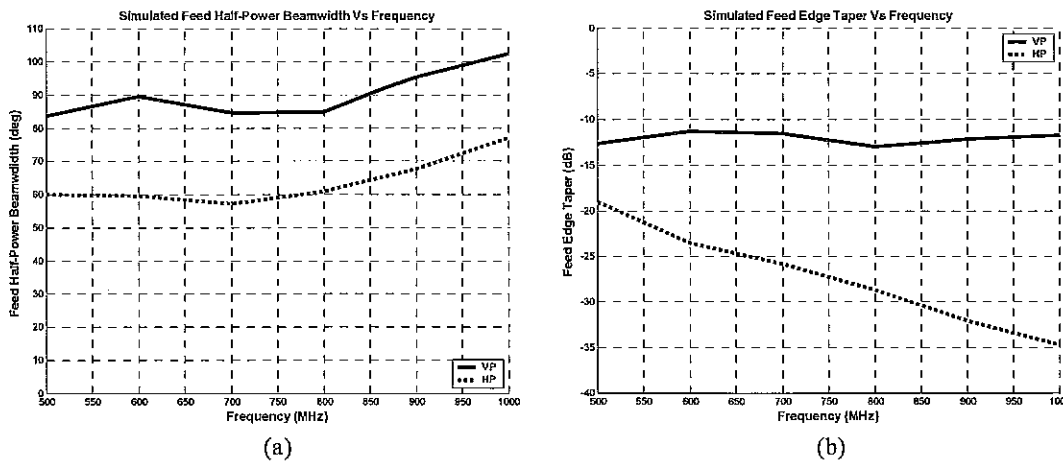


Figure 6.8 Parameter vs. frequency for vertical (VP) and horizontal (HP) polarisations. (a) HPBW. (b) Edge taper.

Co- and cross-polar radiation patterns are shown in Figures 6.9(a) and 6.9(b) for the two polarisations. Cross-polar levels for vertical polarisation are < -36 dB below the co-polar peak at 0° azimuth angle and are negligible. Radiation patterns for the vertical polarisation exhibit minimal variation across the frequency range, with low back radiation, F/B > 26 dB and high polarisation purity within the subtended half-angle range. Patterns for horizontal polarisation in Figure 6.9(b) have narrower beamwidths,

corresponding to reduced aperture efficiency. Sidelobes appearing across the frequency range for azimuth angles around 110° are common for narrow beamwidth patterns, as described in Section 5.5.1. Similar sidelobes are shown in the pattern with a feed beamwidth of 50° , as shown in Figure 5.11. Because these sidelobes are outside the subtended half-angle range, they are not collected by the reflector and hence contribute to an increase in spillover temperature. Back radiation and cross-polar radiation levels are higher than those for the vertical polarisation. The XPR across the frequency range for vertical and horizontal polarisations are shown respectively in Figures 6.10(a) and 6.10(b). The XPR is higher for the horizontal polarisation due to the narrower co-polar feed patterns having a larger edge taper, which reduces the gain gap between the co- and cross-polar patterns. Whereas the co-polar patterns for the vertical polarisation are broader and have a smaller taper resulting in a larger gain gap between the co- and cross-polar patterns.

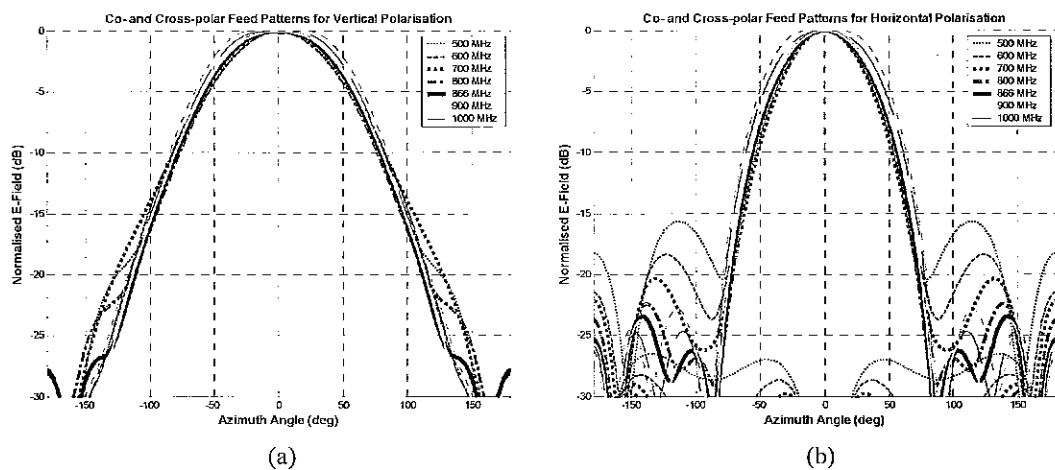


Figure 6.9 Simulated co- and cross-polar patterns at 0° scan angle across the frequency range 500–1000 MHz. (a) Vertical polarisation. * (b) Horizontal polarisation.

*Note cross-polar levels are < -30 dB. The subtended half-angle range for the MOST is $\pm 88^\circ$.

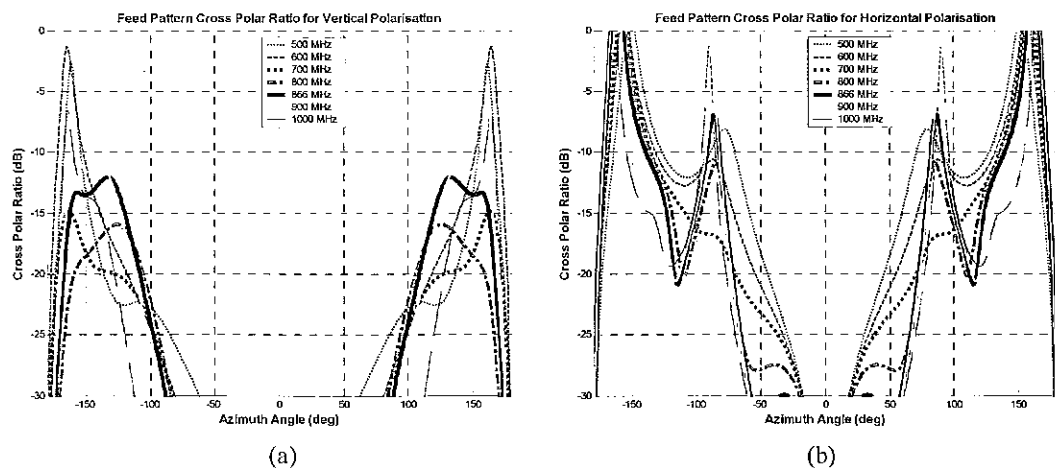


Figure 6.10 Simulated cross-polar ratio. (a) Vertical polarisation. (b) Horizontal polarisation. The subtended half-angle range for the MOST is $\pm 88^\circ$.

The simulated wideband dipole line feed configuration does not meet the feed beamwidth and F/B specifications for the horizontal polarisation. The indifferent performance of the horizontal compared to the vertical polarisation is attributed to the edge effects from the finite ground plane width. For the horizontal polarisation, currents generated on the

ground plane are directed in the plane transverse to the feed length and 'see' a finite edge. When these currents encounter the finite edge, they scatter and their polarisation is no longer strictly in the same orientation as the dipole arm currents. These edge currents cause a reduction in beamwidth and degradation in cross-polar and back radiation levels. They are lower for the vertical polarisation because the ground plane currents generated in this case flow in the longitudinal direction which is continuous rather than finite. The currents remain in the same orientation as dipole arm currents and do not have a significant effect on the transverse plane pattern. Although a different polarisation orientation such as dual slant could improve certain aspects of the radiation performance, the corresponding patterns are asymmetric when the feed is scanned because the polarisations are not aligned with the scanning plane. A line feed tuning methodology is necessary to minimise the ground plane edge effects for the horizontal polarisation, thereby improving its transverse pattern performance. Features requiring improvement are the narrow beamwidth, appearance of sidelobes, reduction of back radiation and cross-polar levels.

6.4.2 Transverse Plane Beamwidth Matching

Although the dual linear polarisation configuration has acceptable radiation performance for the vertical polarisation, its performance is degraded for the horizontal polarisation due to edge effects from the finite ground plane. Physically increasing the ground plane width could reduce these edge effects. However, increasing the ground plane width increases the aperture blockage, which leads to a degradation in sensitivity. In fact, the ground plane width is fixed for the current design, as described in Section 3.4.1. A better approach involves modifying the transverse profile of the line feed, so that the magnitude of the edge currents are minimised and the radiation pattern is tuned. The transverse line feed profile can be modified by using ground plane shaping techniques, flanges, channels or rods placed parallel to the array direction. Lindmark et al. (1999) used ground plane shaping techniques, whereas Wong and Luk (2003) used flanges, as described in Section 4.1.3, to reduce the co-polar pattern back radiation in the transverse plane for aperture coupled patch elements. The line feed design described by Kildal (1980) uses metallic rods placed symmetrically either side of a dual linear polarised crossed dipole element aligned parallel to the array direction to modify the transverse polarisation pattern. Two rods were used to provide almost equal patterns on orthogonal polarisations. On axis cross-polar levels were also reduced.

For the present design, the transverse profile of the feed is modified using metallic flanges or channels because they are simple to implement, as shown in Figure 6.11. Goals of this design are to:

- Determine a configuration that increases half-power beamwidth levels for the horizontal polarisation.
- Reduce the sidelobes, back radiation and cross-polar levels for the horizontal polarisation
- Improve the beamwidth match between orthogonal polarisations.

Because the electrical dimensions of the channels are frequency dependent, it will be difficult to maintain matched beamwidths for both polarisations across the 500–1000 MHz frequency range. The approach taken concentrates on matching the beamwidths at the centre frequency, 866 MHz, for 0° scan angle and minimising the beamwidth

variation across the frequency range. A front-to-back ratio level > 25 dB, is used to specify an acceptable back radiation limit.

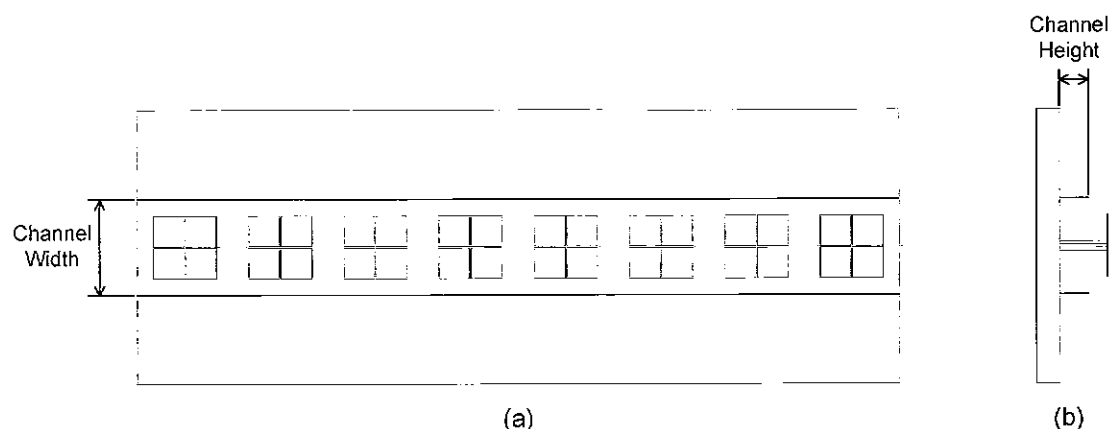


Figure 6.11 Design to reduce the effect of ground plane edge currents on the horizontal polarisation transverse pattern. (a) Top view. (b) End view.

Initial dimensions for the channel were selected as 0.5λ (173 mm) for the width and 0.125λ (43 mm) for the height. Results for the single channel line feed having these dimensions and a discussion are presented in Appendix A.1. Channel height and width dimensions were adjusted in a parameter analysis to investigate whether a configuration could be attained to minimise the beamwidth variation and improve radiation performance at the low frequency band for the horizontal polarisation. Results for this analysis are presented in Appendix A.2, with the channel dimensions adjusted by ± 17 mm with respect to the initial dimensions of 173×43 mm. A summary of the simulated performance of the single channel line feed is presented next.

Adding channels improved the horizontal polarisation radiation pattern and it was shown that certain radiation parameters could be adjusted by changing the channel height and width dimensions. Raising the channel height increased the beamwidth at the lower operating frequency band, resulting in an improved beamwidth match between polarisations. However, the beamwidth match worsened at frequency ranges outside this band, indicating that the change in channel height, 17 mm, was too large. In addition, the F/B levels decreased at lower frequencies for taller channels and these levels were not improved when the channel height was reduced. Broadening the channel width was shown to improve the F/B and reduce the beamwidth for frequencies above 600 MHz. However, the low frequency pattern performance was not affected by a change in channel width. A channel configuration 190 mm wide and 50 mm high produces a horizontal polarisation beamwidth within the 70° – 100° specification across the frequency range. However, the F/B at the lower frequency remained outside the 25 dB specification and the beamwidth difference between orthogonal polarisations was relatively high at 20° .

The limiting parameter of the single channel configuration was the channel height because it had to be raised to increase the beamwidth at the lower frequency, which also increased the back radiation. Although increasing the channel width reduced the back radiation, the improvement was minimal. A new channel configuration was found to improve low frequency F/B and beamwidth performance with the addition of a second 'outer' channel. This configuration is called the dual channel line feed and is shown in Figure 6.12.

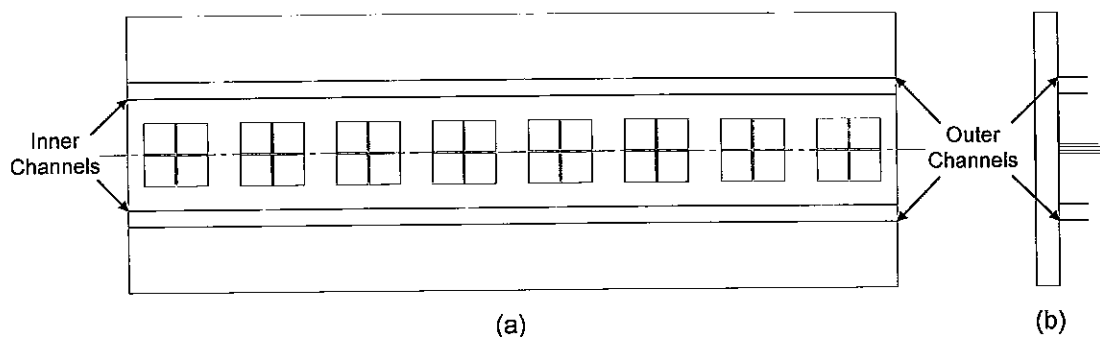


Figure 6.12 Dual channel line feed design showing the inner and outer channels. (a) Top view. (b) End view.

The dual channel analysis begins by choosing the inner channel dimensions, selected to produce low back radiation in a single channel configuration. Initial dimensions were selected for the outer channels and a parameter analysis was again conducted by adjusting these outer dimensions to study the low frequency performance. Appropriate inner channel dimensions were $0.58 \times 0.13\lambda$ (200×45 mm). Initial dimensions for the outer channels were $0.75 \times 0.13\lambda$ (260×45 mm). In the parameter analysis, the inner channels were kept constant and the outer channel dimensions adjusted by $\pm 0.05\lambda$ (17 mm).

Results for this dual channel feed are presented in Table 6.3. The horizontal polarisation beamwidths at the lower frequencies increased to within the 70° – 100° range, as shown in Figure 6.13(a). The edge tapers for orthogonal polarisations are matched within 3 dB across the frequency range 700–1000 MHz. There is an improvement in XPR, shown in Table 6.3, at frequencies < 700 MHz for the horizontal polarisation compared to the single channel feed results in Table A.1. This is because the co-polar beamwidths are increased in the dual channel configuration and there is larger gain gap between the co-polar and cross-polar patterns, as shown in Figure 6.15(b). The beamwidth match between orthogonal polarisations for the dual channel feed is better than for the single channel feed, as shown in Figure 6.14. The average beamwidth variation for the dual channel feed is around 8° and it varies between -3° and $+18^\circ$ over entire 500–1000 MHz range. Vertical polarisation patterns for the dual channel feed are shown in Figure 6.15(a), with the cross-polar levels being < -30 dB. Comparing these patterns with equivalent patterns for the single channel feed (Figure A.3(a)) shows they are similar, except that the co-polar pattern narrows slightly for the dual channel feed at frequencies > 800 MHz. Horizontal polarisation patterns, in Figure 6.15(b), show that the sidelobes and back radiation are reduced at 500 MHz, with the corresponding F/B level meeting the 25 dB limit. The beamwidth difference at 500 MHz is still relatively large, and a parameter analysis was conducted to investigate whether this could be minimised.

Freq (MHz)	Vertical Polarisation				Horizontal Polarisation			
	HPBW (°)	Edge taper (dB)	F/B (dB)	XPR (dB)	HPBW (°)	Edge taper (dB)	F/B (dB)	XPR (dB)
500	90	-12	26	-31	72	-20	25	-10
600	92	-11	32	-36	80	-15	29	-15
700	87	-12	28	-34	89	-14	29	-21
800	85	-14	27	-28	87	-14	29	-28
866	87	-14	29	-26	82	-15	31	-22
900	86	-14	31	-25	81	-15	32	-20
1000	83	-15	32	-29	80	-15	34	-20

Table 6.3 Dual channel line feed element parameters for vertical and horizontal polarisations with inner channel dimensions: 200×45 mm and outer dimensions: 260×45 mm.

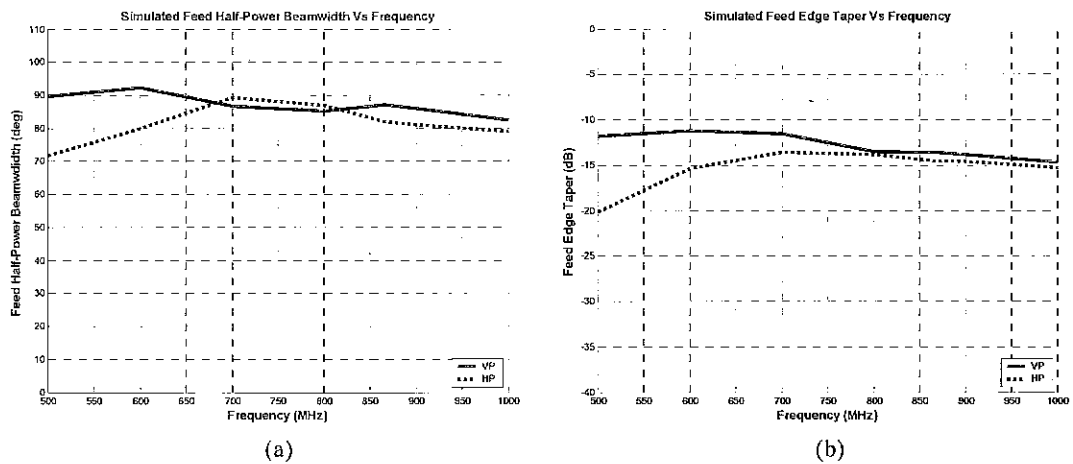


Figure 6.13 Parameter variation with frequency in vertical and horizontal polarisations for dual channel feed. (a) HPBW. (b) Edge taper.

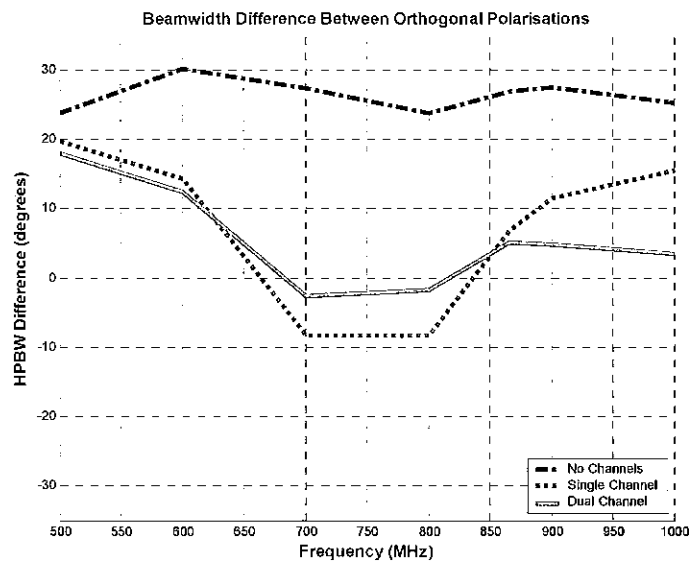


Figure 6.14 Simulated half-power beamwidth difference between orthogonal polarisations for configurations: no channels, single channel (190×50 mm) and dual channel (200×45 mm and 260×45 mm).

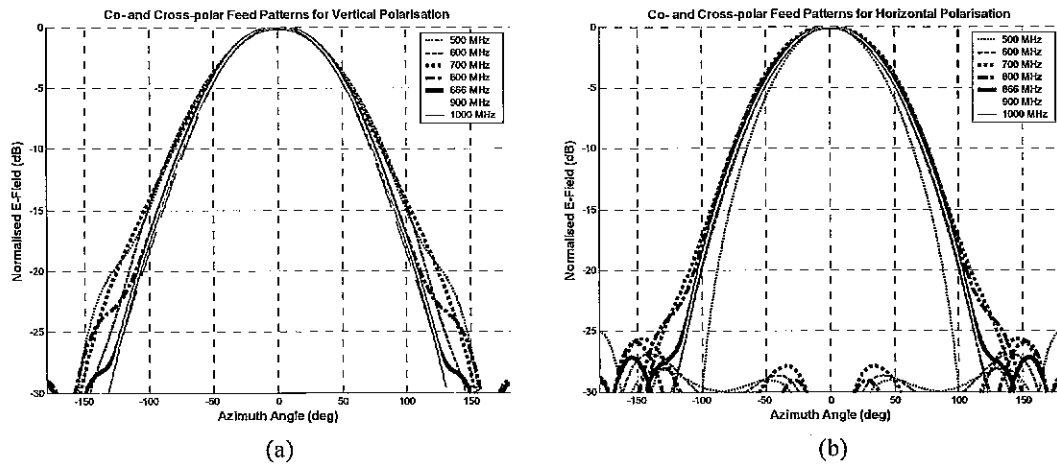


Figure 6.15 Simulated co- and cross-polar patterns at 0° scan angle across 500–1000 MHz for the dual channel line feed. (a) Vertical polarisation.* (b) Horizontal polarisation.

*Note cross-polar levels are < -30 dB. The subtended half-angle range for the MOST is $\pm 88^\circ$.

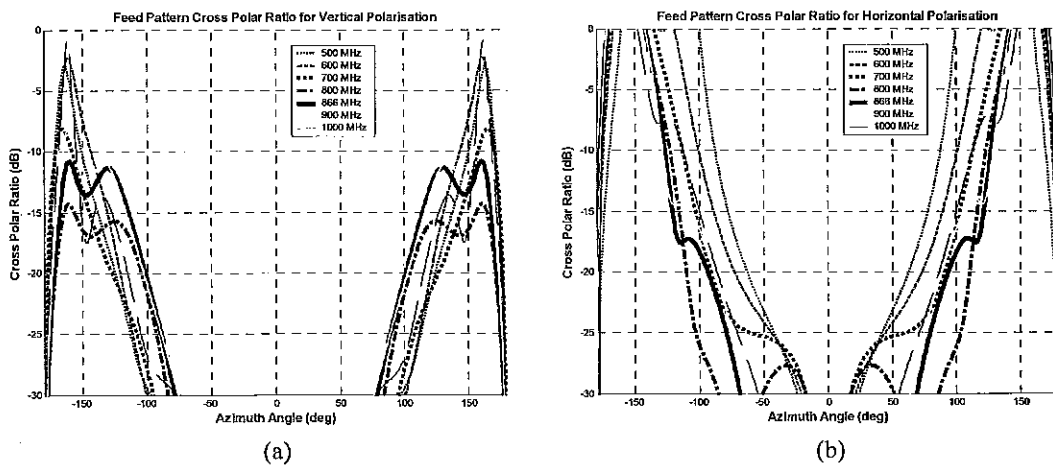


Figure 6.16 Simulated cross-polar ratio for the dual channel line feed (a) Vertical polarisation. (b) Horizontal polarisation. The subtended half-angle range for the MOST is $\pm 88^\circ$.

In the dual channel feed parameter analysis, the inner channel dimensions were kept constant at 200×45 mm and the outer channel height and width dimensions were adjusted by ± 17 mm (0.05λ) to determine whether the beamwidth match at 500 MHz could be improved. The outer channel dimensions were adjusted with respect to the initial dimensions of 260×45 mm. The results for this analysis are presented in Appendix B.

The channel parameter analysis shows that the beamwidth match at 500 MHz is improved by raising the outer channel height. However, the back radiation levels increased at the lower frequency range, with the F/B levels being outside the 25 dB specification for frequencies < 725 MHz. Therefore a trade-off exists between an improved beamwidth match and decreased F/B levels for an increase in channel height for the dual channel feed. Increased back radiation cannot be calibrated in the signal processing. Although a large difference in beamwidth between orthogonal polarisations is undesirable, this effect can be corrected in the signal processing. Rather than selecting a set of optimum dual channel feed dimensions from the subsequent parameter analysis, these results can be used to fine tune the feed radiation performance for a desired frequency range once measured results from the SKAMP Rapid Prototyping Telescope

are obtained. Dual channel dimensions of 200×45 mm for the inner channel and 260×45 mm for the outer channel have been adopted for the initial prototype.

6.4.3 Transverse Element Pattern Scanning Performance

The element pattern scanning performance of the dual channel line feed, is shown in Figures 6.17 to 6.20. Co- and cross-polar element patterns for vertical and horizontal polarisation for 500–1000 MHz at 0° scan angle is shown in Figure 6.15 and for a scan angle range of 15° – 60° in Figures 6.21 to 6.24.

The beamwidth variation over the frequency range for different scan angles is shown for vertical and horizontal polarisations in Figures 6.17(a) and 6.17(b). Beamwidths for the vertical polarisation are within the 70° – 100° limit in the scan angle range from 0° – 30° . For a 45° scan angle, the vertical polarisation half-power beamwidth increases to around 125° at 600 MHz. When the scan angle is increased to 60° , the beamwidth is above the 100° limit across a 525–850 MHz frequency range and increases to 180° at 600 MHz. However, Figure 6.17(a) only shows beamwidths up to 140° to enable easy comparison with the results for the horizontal polarisation beamwidths in Figure 6.17(b). Horizontal polarisation beamwidths are within the 70° – 100° specification across the scan angle range, and show less variation for scan angles $> 45^\circ$ than the beamwidths for the vertical polarisation. The back radiation is increased as the scan angle is increased, for both vertical and horizontal polarisations, as shown in Figures 6.18(a) and 6.18(b), as seen by a reduction in F/B levels. These levels are significantly lower at 60° scan angle for the vertical polarisation compared with the horizontal polarisation, at frequencies < 700 MHz. The edge taper for horizontal and vertical polarisations, shown in Figures 6.19(a) and 6.19(b), are similar at -15 to -12 dB for frequencies between 800–1000 MHz across a scan angle range of 0° – 45° . Figure 6.20 shows that the beamwidth difference between orthogonal polarisations increases substantially for scan angles $> 45^\circ$.

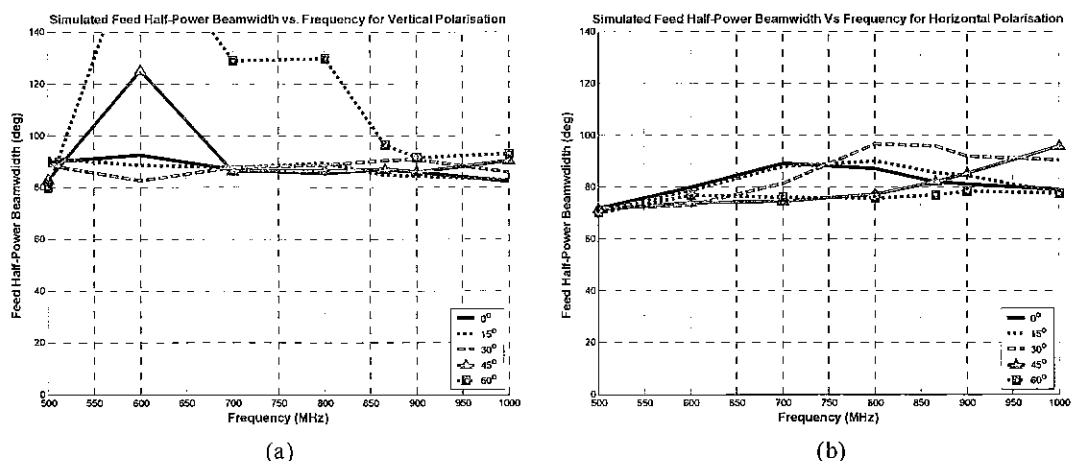
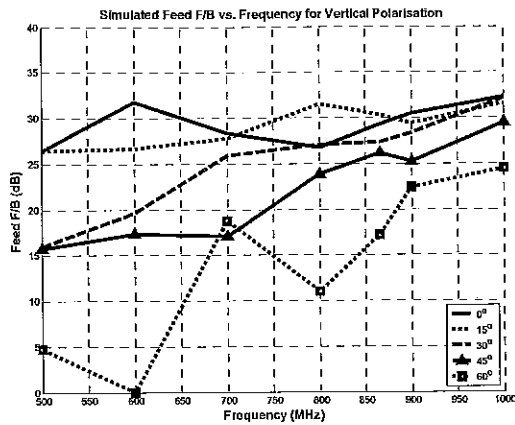
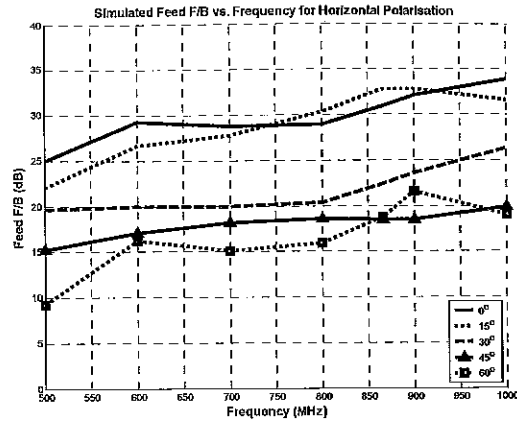


Figure 6.17 Simulated HPBW vs. frequency for dual channel feed over 0° – 60° scan angle. (a) Vertical polarisation.* (b) Horizontal polarisation.

*Note maximum beamwidth is 180° at 600 MHz for a 60° scan angle.

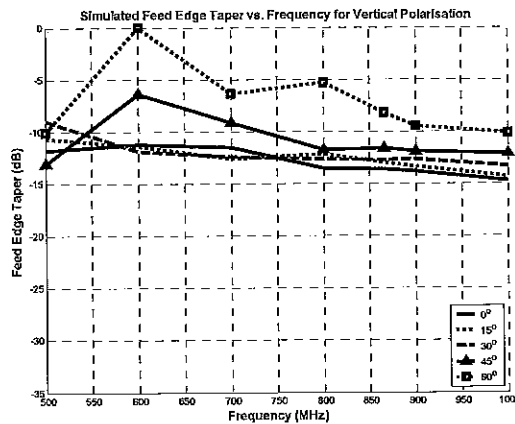


(a)

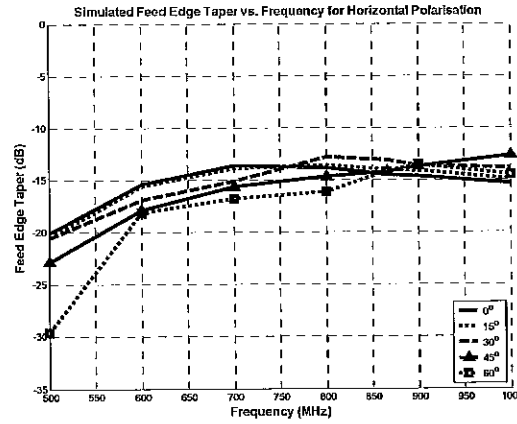


(b)

Figure 6.18 Simulated front-to-back ratio for dual channel feed over 0° – 60° scan angle. (a) Vertical polarisation. (b) Horizontal polarisation.



(a)



(b)

Figure 6.19 Simulated edge taper vs. frequency for dual channel feed over 0° – 60° scan angle. (a) Vertical polarisation. (b) Horizontal polarisation.

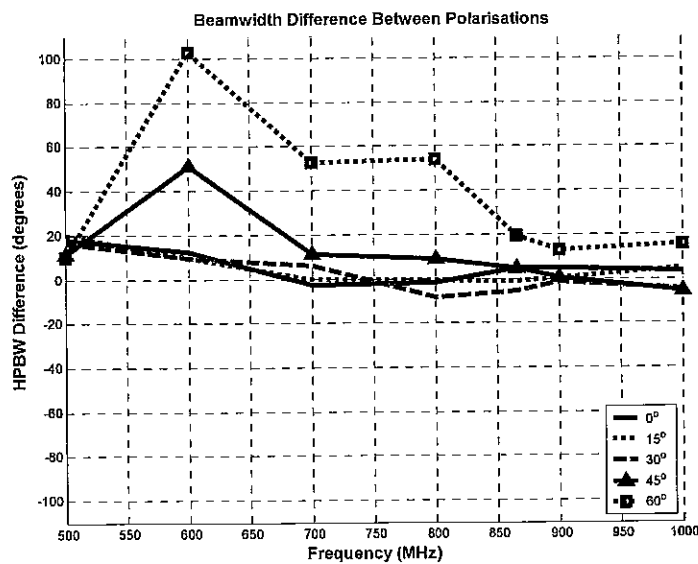


Figure 6.20 Simulated HPBW difference between orthogonal polarisations vs. frequency for dual channel feed over 0° – 60° scan angle.

Co- and cross-polar patterns across the 15° – 60° scanning range are shown in Figures 6.21 to 6.24 for both vertical and horizontal polarisations. These results show the co-polar patterns remain symmetric about the main beam as the scan angle changes, ensuring no beam skewing and asymmetry in the reflector pattern. However, cross-polar and back radiation levels increase at large scan angles on both polarisations and are worse for the vertical polarisation. The increased pattern degradation for the vertical polarisation is due to its orientation on the line feed ground plane. Because the electric field of the vertical polarisation is aligned in the scanning direction, coupling effects from surrounding elements are more significant than when the electric field is aligned orthogonal to the scanning direction, as for the horizontal polarisation. Out-of-phase currents are generated on surrounding elements which create standing waves along the array direction and lead to an increased beamwidth, back radiation and cross-polar levels. This pattern degradation is more prominent at lower frequencies, where the electrical spacing between elements is decreased, and large scan angles, where the coupling effects are greater. These effects are worst in Figure 6.24(a) for frequencies at 500 and 600 MHz for 60° scan angle, where broadening of the co-polar beam and increasing cross-polar levels indicate that resonances are occurring due to feed coupling. Tuning methods to improve the pattern performance at large scan angles for the lower frequency range are limited because mutual coupling is unavoidable and is characteristic of the array geometry.

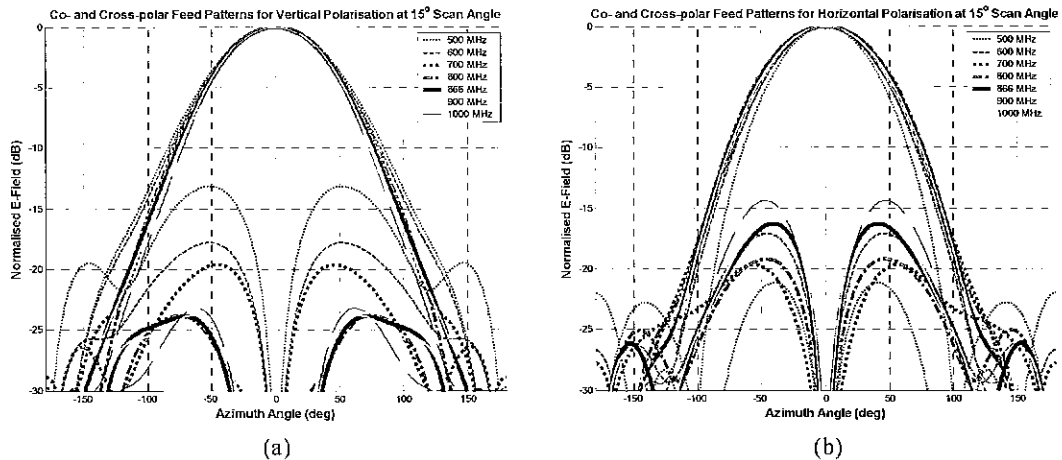


Figure 6.21 Simulated co- and cross-polar patterns at 15° scan angle for 500–1000 MHz for dual channel line feed. (a) Vertical polarisation. (b) Horizontal polarisation.

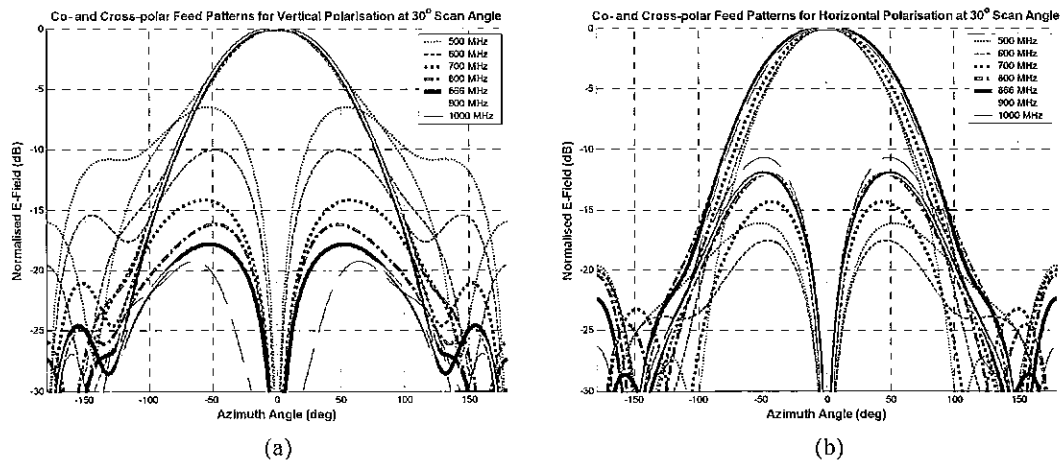


Figure 6.22 Simulated co- and cross-polar patterns at 30° scan angle for 500–1000 MHz for dual channel line feed. (a) Vertical polarisation. (b) Horizontal polarisation.

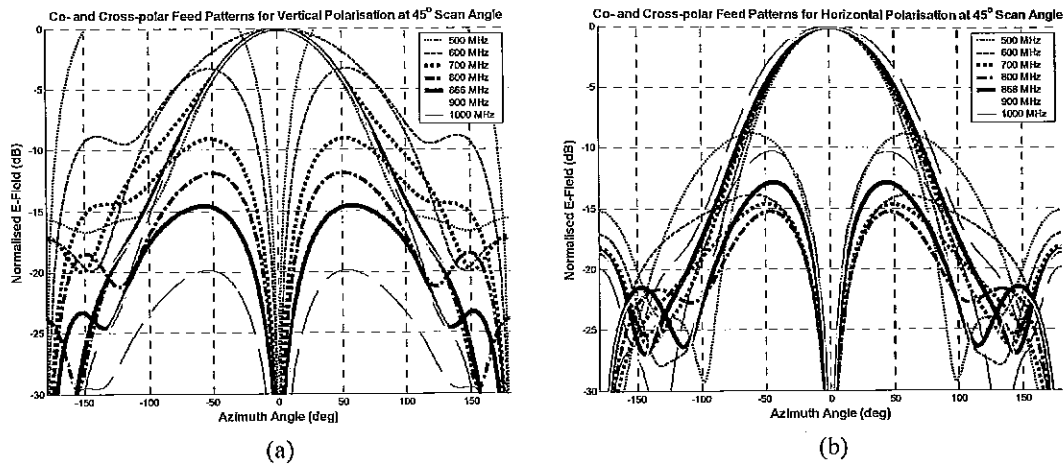


Figure 6.23 Simulated co- and cross-polar patterns at 45° scan angle for 500–1000 MHz for dual channel line feed. (a) Vertical polarisation. (b) Horizontal polarisation.

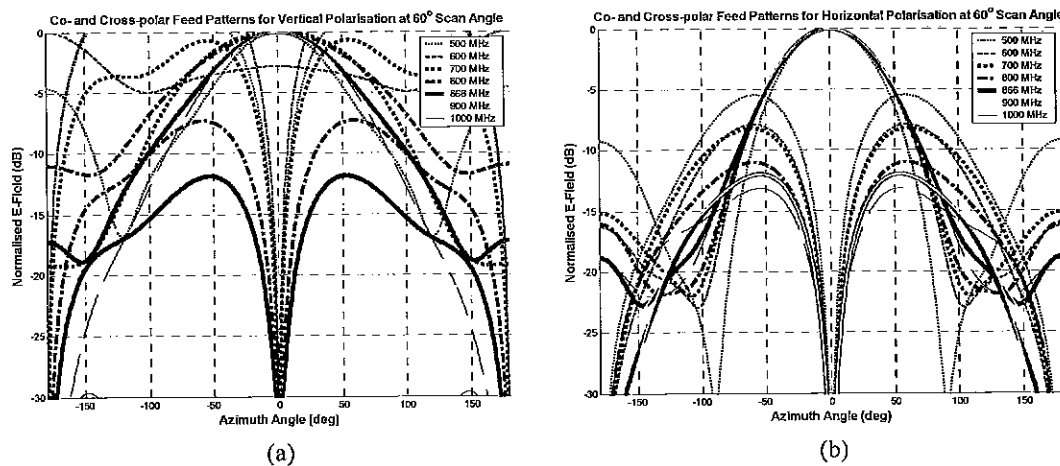


Figure 6.24 Simulated co- and cross-polar patterns at 60° scan angle for 500–1000 MHz for dual channel line feed. (a) Vertical polarisation. (b) Horizontal polarisation.

From the simulated pattern results, acceptable dual channel feed performance occurs for scan angles $< 45^\circ$. Furthermore, the increase in beamwidth difference at 600 MHz, at 45° scan angle, limits the operating frequency range to 700–1000 MHz, for which there is a maximum of $\pm 12^\circ$ beamwidth variation. The F/B limit across this range is 17 dB, occurring at 700 MHz for the vertical polarisation. Operation of this feed at scan angles $> 45^\circ$ is possible but there will be pattern degradation for the vertical polarisation at lower frequencies.

6.4.4 Longitudinal Plane Element Patterns

Element patterns taken along the longitudinal plane, shown in Figure 6.5, represent the gain variation due to scanning the line feed in this plane, as described in Section 6.1.1. When element patterns are taken along the plane of scan for a phased array they are known as scan element patterns (Hansen 1998) and this terminology is used in this thesis, to avoid confusion with the element pattern in the transverse plane described in Section 6.4.2. The scan element patterns will be used to obtain a set of calibration curves to correct for the gain variation with scan angle at selected operating frequencies.

A dual channel feed with the initial channel dimensions: 200×45 mm for the inner channels and 260×45 mm for the outer channels was used in the simulations. The element patterns are obtained from the simulated results for the 8-element module used to obtain the transverse plane patterns (Section 6.4.2), with a radiation pattern cut along the longitudinal or scanning plane. The pattern is displayed in the CST Microwave Studio far-field viewer by selecting the angular coordinates corresponding to a two-dimensional cut in the longitudinal plane. Scan element patterns were obtained at 100 MHz intervals across the 500–1000 MHz frequency range and at the centre frequency 866 MHz, as shown in Figures 6.25(a) and 6.25(b). The scan element patterns in Figure 6.25 are normalised to the peak gain at the particular frequency and the effect of impedance variation is not included. This effect is modelled separately and presented in Section 6.4.6.

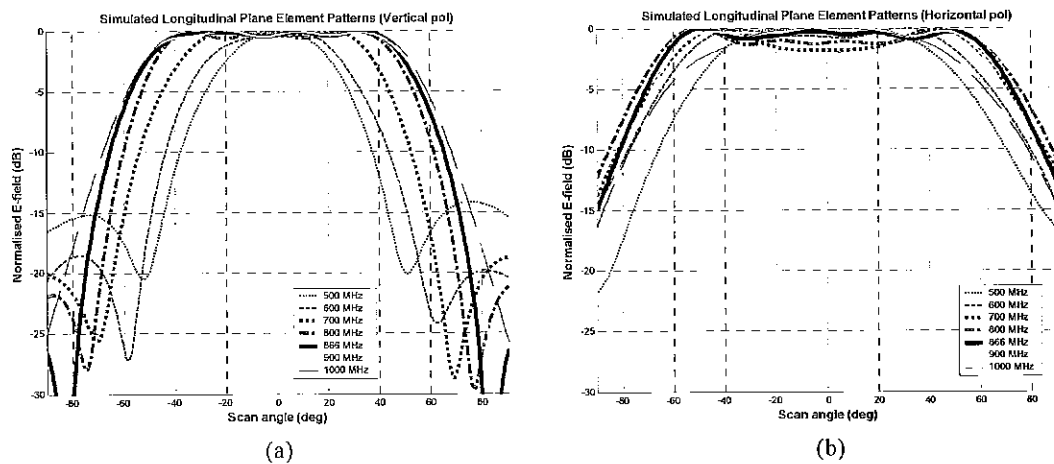


Figure 6.25 Simulated scan element patterns across the 500–1000 MHz range. (a) Vertical polarisation. (b) Horizontal polarisation.

Cross-polar levels for both polarisations are < -30 dB across the scan angle range. This agrees with results obtained for the transverse plane element patterns at 0° azimuth angle, as shown in Figures 6.15 and 6.21 to 6.24. The scan element patterns are different for the two orthogonal polarisations because their orientations are not symmetric with respect to the centre of the ground plane. This gain difference between polarisations is of secondary importance because it will be corrected in the calibration. The important parameter is the gain variation with scan angle at frequencies across the operating band. This parameter will determine the amount of gain reduction caused by the feed pattern and highlight scan angles at which resonances or blind angles occur due to mutual coupling. Scan element patterns for the vertical polarisation, in Figure 6.25(a), are more tapered than the horizontal polarisation, in Figure 6.25(b).

Nulls appearing at 500 MHz for a 50° scan angle and at 600 MHz for a 60° scan angle in the vertical polarisation scan element patterns indicate blind angles and degradation in the transverse plane radiation pattern performance. This is consistent with Figures 6.23(a) and 6.24(a), which show an increase in cross-polar levels and broadening of the co-polar beamwidth for 45° and 60° scan angles at the same frequencies. The co-polar gain reduces to -15 dB at the scan angle limit of $\pm 60^\circ$, indicating a 0.82 gain reduction for frequencies below 700 MHz. A satisfactory result would be 6 dB reduction in co-polar gain at the scan angle limits. Using this constraint, the scan angle range for the vertical polarisation is limited to $\pm 45^\circ$ across a frequency range of 700–1000 MHz. There are no

nulls in the $\pm 60^\circ$ scan region for the horizontal polarisation (Figure 6.25(b)) and there is a smaller gain variation compared to the vertical polarisation. The co-polar gain at 500 MHz reduces to -7.5 dB of the peak at the scan region limits. The frequency range over which there is a 6 dB reduction in co-polar gain, for scan angle limits of $\pm 60^\circ$, is 600–1000 MHz.

Scan element patterns for both vertical and polarisations are asymmetric in Figure 6.25, particularly outside the $\pm 60^\circ$ scan region. This asymmetry is due to the feeding of a central element in an even numbered array required for the element pattern measurement. The array geometry is not symmetric in the longitudinal plane about the central fed element. This is a minor effect occurring predominately at very large scan angles. There are small gain ripples at certain frequencies, for both polarisations, within the flat part of the scan element pattern curve or between the HPBW points. These are due to mutual coupling from surrounding elements and the periodicity of the array geometry. These ripples are similar to periodic grating type responses seen in a microwave filter. The gain ripple magnitude in the scan element pattern depends on the number of array elements and reduces as the number increases. The scan element patterns show that the scanning performance of the feed out to the planned $\pm 60^\circ$ scan angle range will be limited by the pattern nulls and a decrease in gain at large scan angles for the vertical polarisation at frequencies < 600 MHz. The scan angle range for a 6 dB gain reduction is limited to around $\pm 45^\circ$ at 700 MHz for the vertical polarisation. The remaining design study will concentrate on analysing the feed performance in the 700–1000 MHz frequency range and $\pm 45^\circ$ scan angle range.

6.4.5 Single Element Impedance Modelling

In the planned radio frequency (RF) front-end architecture for SKAMP, a low noise amplifier (LNA) is connected to each feed element and polarisation, as described in Section 3.1. For testing purposes, the input impedance of the LNA, Z_{LNA} , will be set to 50Ω . An impedance model for the wideband feed is required in order to determine the mismatch with the LNA. The return loss represents the ratio of reflected signal to received signal due to this mismatch, for a particular frequency. Once the feed impedance has been obtained, a matching network can be designed to reduce the mismatch and improve the return loss.

Firstly, the impedance for a single element in isolation is estimated. The in-pairs feeding network described in Section 6.3.2 is depicted in a circuit diagram in Figure 6.26, showing the feed paths for the two dipoles. The antenna impedance and reference impedance are represented by Z_{ant1} and Z_1 for feed path 1 and Z_{ant2} and Z_2 for feed path 2. The antenna impedance is the simulated impedance at the dipole arm feed point. The in-pairs feeding network is normalised to the reference impedance (Z_{ref}). The reference impedance refers to the impedance that the component is designed to operate at. If the two reference impedances, Z_1 and Z_2 are considered in parallel, then the sum of these impedances is equal to the reference impedance of the LNA, Z_{LNA} equal to 50Ω , giving:

$$Z_{\text{LNA}} = \frac{Z_1 Z_2}{Z_1 + Z_2} \quad (6.7)$$

Assuming equal-amplitude and in-phase feeding makes $Z_1 = Z_2 = Z_{ref}$. Using this identity and Equation 6.7, the reference impedance is calculated as 100Ω , which was used as the reference impedance in the simulation model. Because an equal-amplitude and in-phase feeding is assumed, the antenna impedances Z_{ant1} and Z_{ant2} are equal and the same matching network can be used for both feed paths.

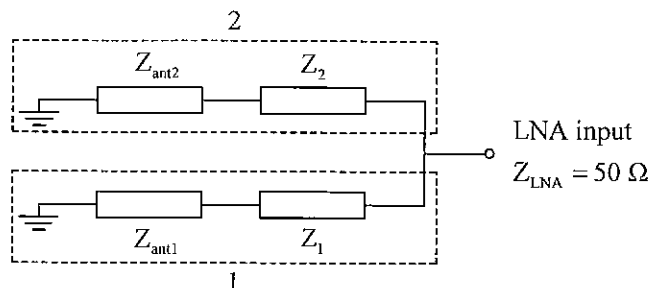


Figure 6.26 Circuit diagram of the in-pairs feeding network.

The impedance model used to obtain the antenna impedance Z_{ant} , was input to CST Microwave Studio, as shown in Figure 6.27. In the model, the metal was represented as a perfect electrical conductor and dielectrics were omitted, to reduce simulation time. To generate in-pairs feeding, a feed strip was used to connect the arms and fed by an s-parameter port, allowing the return loss at the feed point to be calculated. This feeding technique differs from that used in the element pattern model shown in Figure 6.6(b), where only a single port was required to generate the in-pairs feeding. In a parameter analysis of the feed strip width, no significant variation in antenna impedance occurred for widths in the range 0.5–4 mm, so a 2.5 mm strip was used. In the calculations, a solver accuracy of -50 dB was used for the time domain simulations.

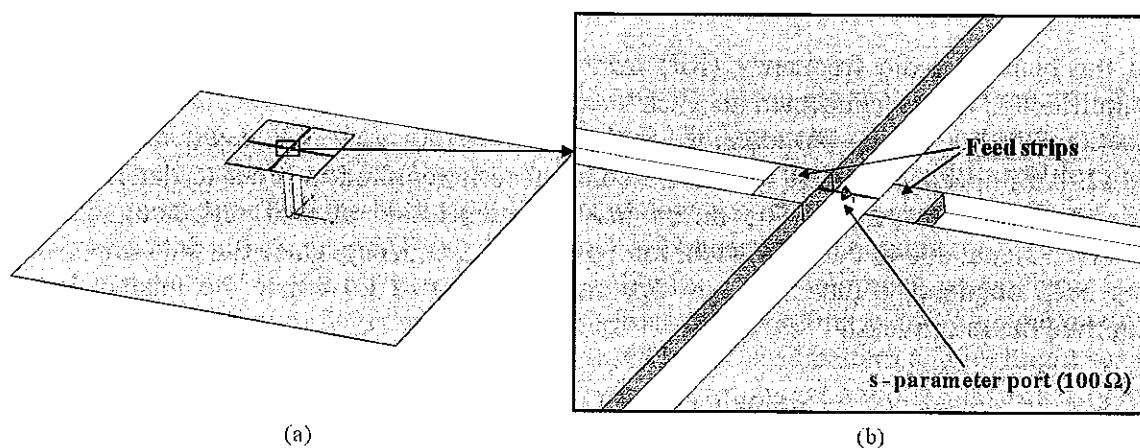


Figure 6.27 CST Microwave Studio model to obtain the antenna impedance at the feed point. (a) Single element on a ground plane. (b) Zoomed in view of the in-pairs feeding technique with the single (s-parameter) excitation port referenced to 100Ω .

The simulated antenna input impedance locus across a frequency range of 500–1400 MHz is shown on a Smith chart plot in Figure 6.28, referenced to a 100Ω impedance. The markers f_L and f_U represent the impedance at the limits of the 700–1000 MHz frequency range. The impedance at the centre frequency, f_c (866 MHz), is $23.0 + j0.8 \Omega$. There is a cross (\times) in the figure at $r = 0.5$, which indicates the 50Ω impedance point, to compare the mismatch with the antenna impedance. The plot shows a matching network is required to reduce mismatch. The accuracy of the impedance model is verified against

measured results from a wideband feed prototype. These measurements and the matching network design are presented in Section 7.1.2.

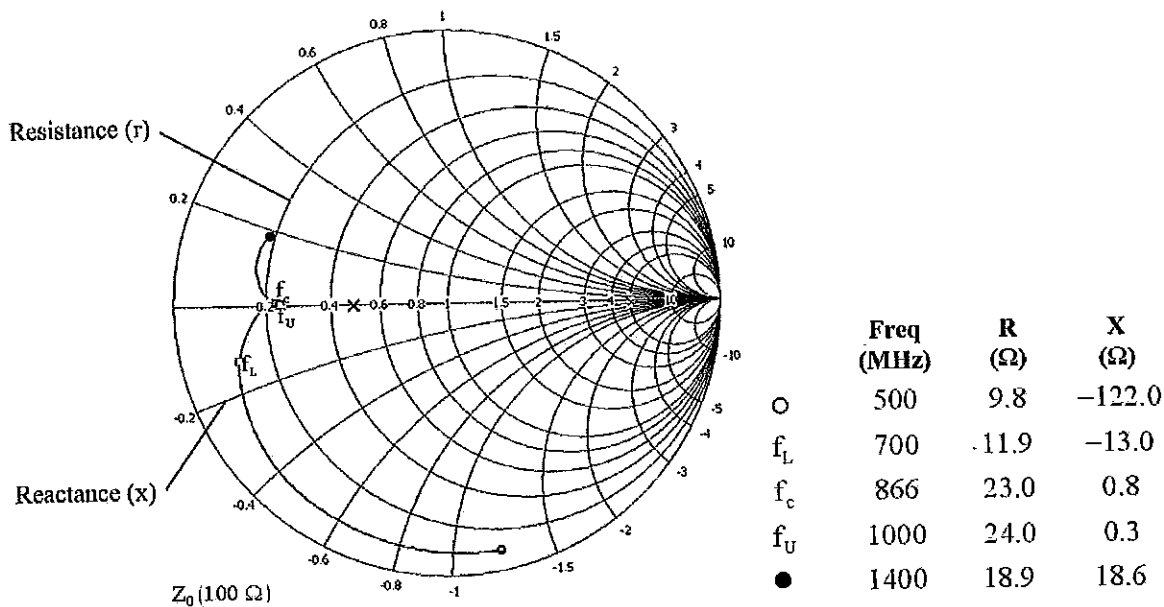


Figure 6.28 Smith chart of the impedance locus at the wideband dipole feed point across 500–1400 MHz band, referenced to 100 Ω from the in-pairs feeding.

*Note: the Smith Chart is referenced to 100 Ω, therefore the 50 Ω impedance circle is $r = 0.5$ ($r = R/100$) and the $Z_0 = 50$ Ω point is marked with an ×.

6.4.6 Scan Impedance Modelling

A model for the scan impedance, $Z_s(\theta)$, was developed to evaluate the wideband dipole at the feed point across the 0°–45° scan angle range, which will be indicative of the array performance. In the simulation model, a unit-cell technique was used and periodic boundary conditions enforced at the two opposite boundaries in the array direction at a distance corresponding to the element spacing. The unit-cell approach assumes that the array is infinite in the direction normal to the periodic boundaries. A scan angle was applied at the periodic boundary to simulate the condition where all elements are phased for a particular direction, as represented in Figure 6.1(a) and a frequency domain solver was used. Simulated scan impedance across 0°–45° scan angle and 700–1000 MHz frequency ranges are shown in Figure 6.29 for vertical polarisation and in Figure 6.30 for horizontal polarisation. Plots show the resistance (R_s) and reactance (X_s) separately, which combine to give the impedance $Z_s = R_s + jX_s$.

Compared to the single element impedance at 866 MHz calculated in Section 6.4.5 to be $Z_{ant} = 23.0 + j0.8$ Ω, the scan element impedances at 0° at the corresponding frequency for vertical and horizontal polarisations were $Z_{VP} = 48.0 + j21.0$ Ω and $Z_{HP} = 23.0 + j22$ Ω. There is a greater difference for scan resistance on the vertical polarisation because it is aligned in the array direction, which increases inter-element coupling. The scan resistance for the vertical polarisation (Figure 6.29(a)) varies from 0–50 Ω across the scan angle and frequency ranges and goes to zero at 30° scan angle for 700 and 900 MHz. This indicates a resonance may occur at these particular frequencies because the impedance mismatch factor in Equation 6.2 becomes zero. The scan resistance for the

horizontal polarisation (Figure 6.30(a)) varies from 0–70 Ω across the scan angle and frequency ranges. The scan resistance again goes to zero at 700 MHz for a 30° scan angle. Comparing the scan resistance and scan reactance at 0° to the corresponding results at 30°, most frequencies show a large variation. This may indicate that a standing wave is generated between the dipole arms and ground plane at this scan angle, which would increase the impedance variation. Another explanation for the large impedance variation could be due to the excitation of an asymmetric mode in the dipole and feed lines (Hansen 1998).

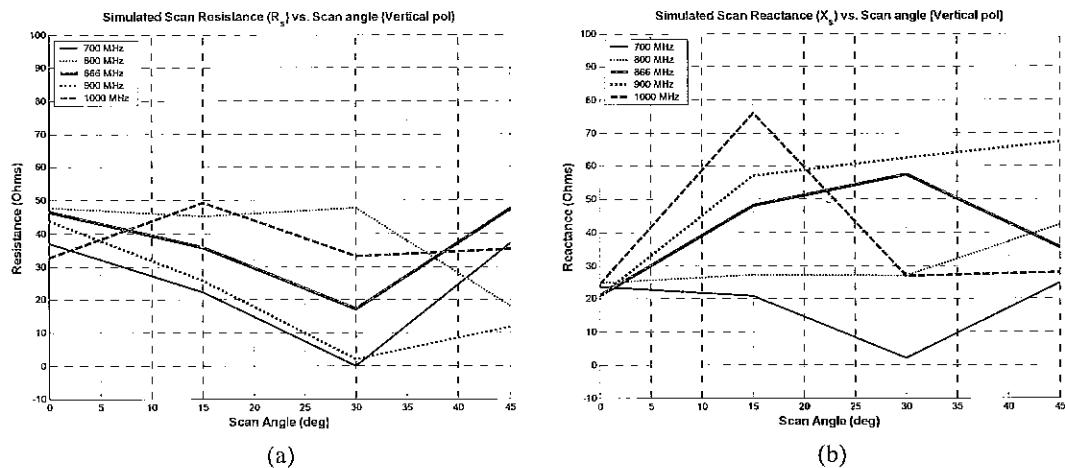


Figure 6.29 Simulated scan impedance for vertical polarisation. (a) Resistance (R_s). (b) Reactance (X_s).

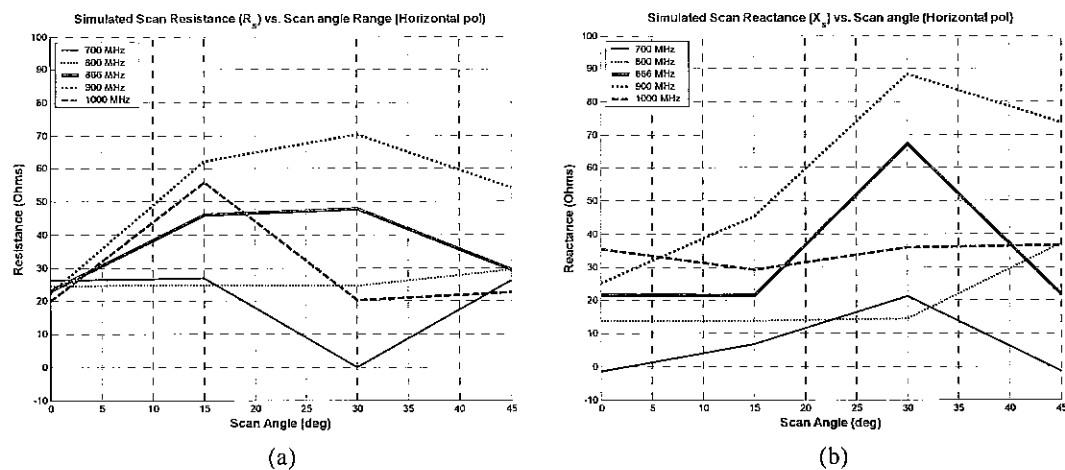


Figure 6.30 Simulated scan impedance for horizontal polarisation. (a) Resistance (R_s). (b) Reactance (X_s).

Ideally the scan resistance and scan reactance for both polarisations should vary minimally to reduce mismatch loss and gain variation. Impedance variation is unavoidable for phased arrays operating over large scan angle ranges due to the increase in mutual coupling. Compensation techniques to minimise the mutual coupling use feed networks, multimode elements and external wave transformers (Hansen 1998), which are outside the scope of this thesis. The balun is not included in the scan impedance model, but there will be an effect as the feed is scanned. Nevertheless, the results shown in Figures 6.29 and 6.30 will indicate how the feed impedance may vary with scan angle and the possible resonances which may be generated. Specialised measurement apparatus is required to confirm the scan impedance model and to characterise the balun.

6.5 Summary

The detailed design of the line feed was described. Array analysis methods used to characterise the radiation and impedance performance are described in Section 6.1. A brief summary of the electromagnetic software used for the line feed design is presented in Section 6.2. Different dual linear wideband dipole array configurations are analysed to determine the optimum configuration for SKAMP. A configuration that consists of arraying the dipoles along the arm width dimension provides greater separation between elements compared to the other configurations presented in Section 6.3.1. Current dual linear dipole designs usually feed the two polarisations along the diagonals of the dipole arms, whereas the selected line feed configuration required feeding the polarisations along the dipole arm width. This led to the development of a new novel in-pairs feeding technique, described in Section 6.3.2.

Element pattern simulations of the line feed, using the in-pairs feeding technique were presented. Transverse plane element patterns simulations showed that the vertical and horizontal polarisation patterns were unequal due to their different polarisation orientations on the ground plane. A beamwidth matching methodology using beam shaping channels for the two polarisations was presented in Section 6.4.2. A dual channel configuration provided the best beamwidth tuning for the horizontal polarisation to attain the beamwidth and F/B specifications and minimise the beamwidth difference with vertical polarisation. However, the beamwidth difference at the lower frequency end, 500 MHz, was still relatively large at 18° . The scanning performance of the dual channel line feed was investigated in Sections 6.4.3 and 6.4.4. Evaluation of the adopted feed showed an acceptable operating frequency range of 700–1000 MHz with a $\pm 45^\circ$ scan angle range. An impedance simulation of a single element, in Section 6.4.5, showed a matching network is required to improve its return loss. A scan impedance model presented in Section 6.4.6 was used to analyse the impedance variation with scan angle, with simulations showing the presence of potential standing waves occurring at 700 and 900 MHz for a 30° scan angle.